

An improved reproducing Hilbert kernel method to solve the model of neutron transporting process in nuclear reactor core

Ming-Jing Du(杜明婧), Bao-Jun Sun(孙宝军), Yin-Feng Chen(陈银凤), Ge Kai(凯歌)

Citation: Chin. Phys. B. 35, 090209 (2026). DOI: 10.1088/1674-1056/ae181d | CSTR: 32038.14.CPB.ae181d

http://cpb.iphy.ac.cn; http://iopscience.iop.org/cpb

What follows is a list of articles you may be interested in

Probabilistic distribution and stochastic P-bifurcation of a nonlinear energy-regenerative suspension system with time-delayed feedback control

Zhao-Bin Zeng(曾昭彬), Ya-Hui Sun(孙亚辉), Yang Liu(刘洋)

Chin. Phys. B. 35, 010201 (2026). DOI: 10.1088/1674-1056/ade669 | CSTR: 32038.14.CPB.ade669

Adaptive multi-step piecewise interpolation reproducing kernel method for solving the nonlinear time-fractional partial differential equation arising from financial economics

Ming-Jing Du(杜明婧), Bao-Jun Sun(孙宝军), Ge Kai(凯歌)

Chin. Phys. B. 32, 030202 (2023). DOI: 10.1088/1674-1056/ac9368

Data-driven parity-time-symmetric vector rogue wave solutions of multi-component nonlinear Schrödinger equation

Li-Jun Chang(常莉君), Yi-Fan Mo(莫一凡), Li-Ming Ling(凌黎明), De-Lu Zeng(曾德炉)

Chin. Phys. B. 31, 060201 (2022). DOI: 10.1088/1674-1056/ac4cc5

A local refinement purely meshless scheme for time fractional nonlinear Schrödinger equation in irregular geometry region

Tao Jiang(蒋涛), Rong-Rong Jiang(蒋戎戎), Jin-Jing Huang(黄金晶), Jiu Ding(丁玖), Jin-Lian Ren(任金莲)

Chin. Phys. B. 30, 020202 (2021). DOI: 10.1088/1674-1056/abc0e0

Improved reproducing kernel particle method for piezoelectric materials

Ji-Chao Ma(马吉超), Gao-Feng Wei(魏高峰), Dan-Dan Liu(刘丹丹)

Chin. Phys. B. 27, 010201 (2018). DOI: 10.1088/1674-1056/27/1/010201

An improved reproducing Hilbert kernel method to solve the model of neutron transporting process in nuclear reactor core

Ming-Jing Du(杜明婧)[1,†], Bao-Jun Sun(孙宝军)[1], Yin-Feng Chen(陈银凤)[1], and Ge Kai(凯歌)[2]

[1] *School of Computer Information Management, Inner Mongolia University of Finance and Economics, Hohhot* 010070, *China*
[2] *School of Statistics and Mathematics, Inner Mongolia University of Finance and Economics, Hohhot* 010070, *China*

(Received 4 September 2025; revised manuscript received 15 October 2025; accepted manuscript online 28 October 2025)

We propose an adaptive double piecewise interpolation reproducing Hilbert kernel method (ADPIRHKM) for the first time to solve the model of the neutron transporting process in the nuclear reactor core. The theory focuses on the reproducing kernel theory, integrated with the adaptive technique and the double piecewise interpolation means, which can produce a sparse matrix B by selecting the appropriate parameters, avoiding calculating the conjugate operator and practising Gram–Schmidt orthogonalization. The adaptive multi-step technique, which ensures a more reasonable segment count, and the double piecewise interpolation approach, which enhances accuracy, combine together to give a key innovation point of this paper: a simple and efficient numerical method. Three numerical experiments are done to show the accuracy of the new method and the comparisons are based on the known results. The numerical simulation indicates the effect of time t and β on neutron flux behavior of graphite.

Keywords: reproducing kernel method, nonlinear time-fractional telegraph equations, adaptive technique, double piecewise interpolation, numerical experiments

PACS: 02.60.Cb, 02.60.–x, 02.30.Jr

DOI: 10.1088/1674-1056/ae181d **CSTR:** 32038.14.CPB.ae181d

1. Introduction

In recent years, the fractional-order telegraph equation has garnered significant attention in both theoretical and applied aspects, and has made substantial advancements. Currently, the fractional-order telegraph equation is utilized in various applied scientific fields to describe a wide range of phenomena, such as fluid flow in porous materials, reaction-diffusion phenomena, sound propagation in the viscoelastic materials, dynamics of self-similar structures, and signal processing in biological electric systems. Due to the inherent characteristics of fractional calculus, its introduction has addressed the shortcomings of classical differential equations in representing objective realities. However, the fractional-order telegraph equations derived from practical problems are often nonlinear variable-coefficient partial differential equations. Most of these problems do not have exact analytical solutions, and generally yield numerical solutions. Therefore, to obtain their analytical forms, numerical methods must be employed for solving them. In Ref. [1], the authors proposed a meshless spectral method for working out the nonlinear time-fractional telegraph equation (TFTE), which employed two main stages to approximate the unknown solution. In Ref. [2], the authors presented two collocation methods made with one-dimensional (1D) and two-dimensional (2D) Romanovski–Jacobi polynomials for solving the nonlinear TFTE. In Ref. [3], Uday Singh introduced a new method for approximating the TFTE using spline functions, which transformed the fractional-order model into a series of algebraic equations that can be solved by using Newton's iterated method. In Ref. [4], the authors addressed the pseudo-hyperbolic telegraph equation involving the Caputo fractional derivative by using an explicit finite difference method. In Ref. [5], Mamta Kapoor provided the particular Lagrange interpolation polynomial DQM and the NUAH B-spline DQM for solving the hyperbolic telegraph equation. In Ref. [6], the authors presented an adaptive Monte Carlo method for solving the telegraph equation. In Ref. [7], Suayip proposed a collocation method for working out the 1D telegraph equation, based on the first kind of Bessel functions. By utilizing operation matrices involving collocation points and derivatives, the nonlinear TFTE was simplified to a set of linear algebraic equations. In Ref. [8], Zogheib and Tohidi introduced a modal Hermite spectral collocation (MHSC) method to work out the multi-dimensional telegraph equations, which incorporated suitable initial time conditions and boundary space conditions to provide numerical solutions.

Notably, the truncated unknown coefficient Hermite series were employed to approximate the solution in both spatial and temporal variables. In Ref. [9], the authors focused on the Vieta–Lucas Tau operational method and applied it to

[†]Corresponding author. E-mail: 724297269@qq.com

© 2026 Chinese Physical Society and IOP Publishing Ltd. All rights, including for text and data mining, AI training, and similar technologies, are reserved.

solve initial value problems. In Ref. [10], a novel numerical method for working out the second-order 2D HTE was proposed, accommodating initial boundary and Dirichlet boundary conditions. In particular, when employing a symmetric Sinc–Galerkin method, the numerical results were very accurate. The more complex nonlinear time-fractional telegraph equation is a widely used model for representing various physical phenomena, such as the propagation of electrical signals in transmission lines, the strange behavior of the complex frequency-dependent processes, and the spread of special diseases and infectious diseases.[11] In this paper, we aim at the numerical simulation of the nonlinear TFTE equation which can be expressed with the Caputo sense. This mathematical model is an effective description of the neutron transporting processes in the core of a nuclear reactor[1]

$$\frac{\partial^{\beta}\Phi(\boldsymbol{r},t)}{\partial t^{\beta}}+\frac{\partial^{\beta-1}\Phi(\boldsymbol{r},t)}{\partial t^{\beta-1}}+\Phi(\boldsymbol{r},t)$$
$$=\Delta\Phi(\boldsymbol{r},t)+P(\Phi(\boldsymbol{r},t))+F(\boldsymbol{r},t),$$
$$\boldsymbol{r}=(r,y)\in\Omega\subset\boldsymbol{R}^2,\ 0<t\le T, \tag{1}$$

with initial conditions and the boundary conditions

$$\Phi(\boldsymbol{r},0)=\varphi(\boldsymbol{r}),\ \frac{\partial\Phi(\boldsymbol{r},0)}{\partial t}=\psi(\boldsymbol{r}),\ r\in\overline{\Omega}=\Omega\cup\partial\Omega, \tag{2}$$
$$\Phi(\boldsymbol{r},t)=\hbar(\boldsymbol{r},t),\ \boldsymbol{r}\in\partial\Omega,\ t>0, \tag{3}$$

where $\Phi(\boldsymbol{r},t)$ is the neutrons, which is the unknown function that we need to find, β is the fractional order where $1<\beta<2$, the symbol Δ is the Laplace operator, $\bar{\Omega}$ represents a spatial domain in r^2 with sequential boundary $\partial\Omega$. The source term $F(\boldsymbol{r},t)$ is a continuously smooth function, and $\varphi(\boldsymbol{r})$, $\psi(\boldsymbol{r})$, and $P(\Phi(\boldsymbol{r},t))$ are continuous functions. The equation can also be one dimension. Next, we define the fractional derivatives in the Caputo sense as

$$\frac{\partial^{\beta}\Phi(\boldsymbol{x},t)}{\partial t^{\beta}}=\begin{cases}\dfrac{1}{\Gamma(m-\beta)}\displaystyle\int_0^t(t-\tau)^{m-\beta-1}\frac{\partial^m\Phi(\boldsymbol{x},\tau)}{\partial\tau^m}\,\mathrm{d}\tau, & m-1<\beta<m,\\ \dfrac{\partial^m\Phi(\boldsymbol{x},t)}{\partial t^m}, & \beta=m\in N.\end{cases} \tag{4}$$

In this study, the authors propose an improved numerical method to simulate the nonlinear TFTEs (1)–(3). As we know, the traditional reproducing Hilbert kernel method (TRHKM) has gained significant traction in various fields, particularly in machine learning, statistics, and functional analysis, due to its strong mathematical foundation and versatility in approximating complex functions. The notion of reproducing kernels allows for a structured approach to infinite-dimensional spaces, enabling the representation of linear functionals and encompassing various applications, from regression problems to classification tasks. In Ref. [12], a novel TRHKM was proposed to show that high-order linear Fredholm integro-differential equations (FIDE) with variable coefficients can be converted into ordinary differential equation (ODE). In Ref. [13], based on reproducing kernel Hilbert space (RKHS) theory, Attia and Akgul solved the fractal fractional differential equations and well numerical results are obtained. In Ref. [14], the authors developed a numerical investigation for Caputo–Fabrizio fractional Bernoulli and Riccati equations by using iterative RHKM. In 2024, the authors of this paper improved the TRHKM by using adaptive technique and single piecewise interpolation technology,[15] achieving a high-precision numerical solution. However, single piecewise interpolation is insufficient for more complex mathematical models. To address this issue, this paper introduces the ADPIRHKM for the first time. The interpolation facilitates a smoother problem configuration, reducing computational errors. By integrating the advantages of adaptive techniques with the high precision of double piecewise interpolation, the number of pieces is minimized while ensuring computational accuracy. Therefore, the research presented in this paper has great significance for solving various types of equations and conducting numerical computations.

This paper is arranged as follows: In Section 2, the series expressions for analytical solution and approximate solution of Eqs. (1)–(3) are obtained by reproducing kernel functions, and the technical route of the ADPIRHKM is given. Three numerical experiments are done in Section 3. The numerical simulation indicates the effect of time t and β on neutron flux behavior of graphite in Section 4. We give a brief conclusion in Section 5.

2. Reproducing kernel Hilbert spaces

For easy elaboration and understanding, we consider the 1D nonlinear TFTE, let $(r,t)\in\Omega=[0,1]\times[0,1]$, the RKHSs and their reproducing kernels (RKs) are given as follows:

(i) The RKHS $\Upsilon_2^1[0,1]=\{r|r$ is one-variable absolutely continuous function, $r'\in L^2[0,1]\}$.

The inner product is defined by

$$\langle \Phi(r)\ ,\ \Psi(r)\rangle_{\Upsilon_2^1} = \Phi(0)\Psi(0) + \int_0^1 \Phi'(r)\cdot\Psi'(r)\mathrm{d}r\ ,\ \ \Phi(r)\ ,\Psi(r)\ \in\ \Upsilon_2^1[0,1].$$

The RK of the $\Upsilon_2^1[0,1]$ is

$$R_r^{\{1\}}(t) = \begin{cases} 1+r,\ t>r, \\ 1+t,\ r>t. \end{cases}$$

(ii) The RKHS $\Upsilon_2^3[0,1] = \{\Phi|\Phi,\Phi',\Phi''$ are one-variable absolutely continuous functions, $\Phi(0)=\Phi'(0)=0, \Phi'''\in L^2[0,1]\}$. The inner product is defined by

$$\langle \Phi(r)\ ,\ \Psi(r)\rangle_{\Upsilon_2^3} = \sum_{k=0}^{2}\Phi^{(k)}(0)\Psi^{(k)}(0) + \int_0^1 \Phi'''(r)\cdot\Psi'''(r)\mathrm{d}r\ ,\ \ \Phi(r)\ ,\Psi(r)\ \in\ \Upsilon_2^3[0,1].$$

The RK of $\Upsilon_2^3[0,1]$ is

$$R_r^{\{2\}}(t) = \begin{cases} r^2(r^3-5r^2t+30t^2+10rt^2)/120,\ t>r, \\ t^2(-5rt^2+t^3+10r^2(3+t))/120,\ r>t. \end{cases}$$

(iii) The RKHS $\Upsilon_{2.0}^3[0,1] = \{\Phi|\Phi,\Phi',\Phi''$ are one-variable absolutely continuous functions, $\Phi(0)=\Phi(1)=0, \Phi'''\in L^2[0,1]\}$. The inner product is defined by

$$\langle \Phi(r)\ ,\ \Psi(r)\rangle_{\Upsilon_{2.0}^3} = \sum_{k=0}^{2}\Phi^{(k)}(0)\Psi^{(k)}(0) + \int_0^1 \Phi'''(r)\cdot\Psi'''(r)\mathrm{d}r\ ,\ \Phi(r)\ ,\Psi(r)\ \in\ \Upsilon_{2.0}^3[0,1].$$

The RK of $\Upsilon_{2.0}^3[0,1]$ is

$$R_r^{\{3\}}(t) = \begin{cases} \dfrac{t(-r(120+30r+10r^2-5r^3+r^4)(120+30t+10t^2-5t^3+t^4+156(t^4+10r^2t(3+t)-5r(t^3-24)))}{18720} \\ \text{with}\ \ t>r, \\ \dfrac{r(156(120t+30rt^2+10r^2t^2-5r^3t+r^4)-(120+30r+10r^2-5r^3+r^4)t(120+30t+10t^2-5t^3+t^4))}{18720} \\ \text{with}\ \ r>t, \end{cases}$$

(iv) The RKHS

$$\begin{aligned} H(\Omega) &= \Upsilon_2^3[0,1]\otimes\Upsilon_{2.0}^3[0,1] \\ &= \Big\{\Phi(r,t)|\frac{\partial^{n+m}}{\partial r^n\partial t^m}\Phi(r,t)\ \text{ are two-variable complete continuous functions}, n=0,1,2,3; m=0,1,2,3, \\ &\qquad \frac{\partial^{p+q}}{\partial r^p\partial t^q}\Phi(r,t)\in L^2(\Omega),\ p=0,1,2,3,\ q=0,1,2,3,\ \Phi(r,0)=\Phi'(r,0)=\Phi(0,t)=\Phi(1,t)=0\Big\} \\ &= \Big\{\Phi(r,t)|\sum_{i=1}^{\infty}\sum_{j=1}^{\infty}c_{ij}\widetilde{y}_1^{(i)}(r)\cdot y_2^{(j)}(t) : \forall\sum_{i=1}^{\infty}\sum_{j=1}^{\infty}|c_{ij}|^2<\infty\Big\}, \end{aligned}$$

where $\widetilde{y}_k^{(i)}$ are complete orthogonal function systems of $\Upsilon_2^3[0,1]$ and $\Upsilon_{2.0}^3[0,1]$. Furthermore,

$$\Phi(r,t) = \sum_{i=1}^{\infty}\sum_{j=1}^{\infty}c_{ij}\widetilde{y}_1^{(i)}(r)\cdot y_2^{(j)}(t)\in H(\Omega),\ y(r,t) = \sum_{i=1}^{\infty}\sum_{j=1}^{\infty}d_{kl}\widetilde{y}_1^{(k)}(r)\cdot y_2^{(l)}(t)\in H(\Omega).$$

The inner product of $H(\Omega)$ is defined by

$$\langle\Phi,y\rangle = \sum_{i=1}^{\infty}\sum_{j=1}^{\infty}\sum_{i=1}^{\infty}\sum_{j=1}^{\infty}c_{ij}\bar{d}_{kl}\left\langle\widetilde{y}_1^{(i)},\widetilde{y}_1^{(k)}\right\rangle_1\left\langle y_2^{(j)},y_2^{(l)}\right\rangle_2 = \sum_{i=1}^{\infty}\sum_{j=1}^{\infty}c_{ij}\bar{d}_{ij},$$

so the RK of $H(\Omega)$ is $R^1_{(\xi,\eta)}(r,t) = R_\xi^{\{3\}}(r)\times R_\eta^{\{2\}}(t)$.

(v) The RKHS

$$H_1(\Omega) = \Upsilon_2^1[0,1]\otimes\Upsilon_2^1[0,1]$$

$$= \left\{ \Phi(r,t) | \Phi(r,t) = \sum_{i=1}^{\infty}\sum_{j=1}^{\infty} c_{ij}\widetilde{y}_1^{(i)}(r)\cdot y_2^{(j)}(t) : \forall \sum_{i=1}^{\infty}\sum_{j=1}^{\infty} |c_{ij}|^2 < \infty, \right\},$$

where $\widetilde{y}_k^{(i)}$ are complete orthogonal function systems of $\Upsilon_2^1[0,1]$.

$$\Phi(r,t) = \sum_{i=1}^{\infty}\sum_{j=1}^{\infty} c_{ij}\widetilde{y}_1^{(i)}(r)\cdot y_2^{(j)}(t) \in H_1(\Omega), \quad y(r,t) = \sum_{i=1}^{\infty}\sum_{j=1}^{\infty} d_{kl}\widetilde{y}_1^{(k)}(r)\cdot y_2^{(l)}(t) \in H_1(\Omega).$$

The inner product of $H_1(\Omega)$ is defined by

$$\langle u,y\rangle = \sum_{i=1}^{\infty}\sum_{j=1}^{\infty}\sum_{i=1}^{\infty}\sum_{j=1}^{\infty} c_{ij}\bar{d}_{kl}\left\langle \widetilde{y}_1^{(i)},\widetilde{y}_1^{(k)}\right\rangle_1 \left\langle y_2^{(j)},y_2^{(l)}\right\rangle_2 = \sum_{i=1}^{\infty}\sum_{j=1}^{\infty} c_{ij}\bar{d}_{ij},$$

so the RK of $H_1(\Omega)$ is $R_{(\xi,\eta)}(r,t) = R_{\xi}^{\{1\}}(r)\times R_{\eta}^{\{1\}}(t)$.

3. Adaptive double piecewise interpolation reproducing Hilbert kernel method

In order to solve the nonlinear TFTE by ADPIRHKM, the nonhomogeneous initial conditions should be converted into homogeneous initial conditions, let $Y(r,t) = \Phi(r,t) - Z(r,t)$, in which $Z(r,0) = \varphi(r)$, $\partial Z(r,0)/\partial t = \psi(r)$, $Z(r,t)$ is not unique, as long as the initial conditions and the boundary conditions of $Z(r,t)$ and $\Phi(r,t)$ are equal, so equations (1)–(3) are as follows:

$$\frac{\partial^{\beta} Y(r,t)}{\partial t^{\beta}} + \frac{\partial^{\beta-1} Y(r,t)}{\partial t^{\beta-1}} + Y(r,t) - \Delta Y(r,t) - P(Y(r,t)) = f(x,t,Y(r,t)),\ 0 < r \le 1,\ 0 < t \le 1, \tag{5}$$

with initial conditions

$$Y(r,0) = 0,\ \frac{\partial Y(r,0)}{\partial t} = 0, \tag{6}$$

and the boundary conditions

$$Y(0,t) = 0,\ Y(1,t) = 0. \tag{7}$$

In Section 2, the RKHSs $\Upsilon_2^1[0,1]$, $\Upsilon_{2,0}^3[0,1]$, $\Upsilon_2^3[0,1]$, $H(\Omega)$, and $H_1(\Omega)$ have been defined. Let

$$(LY)(r,t) = f(r,t,Y(r,t)),$$

where $L: H(\Omega) \to H_1(\Omega)$ is a bounded linear operator, L^* is a bounded linear operator, and the L^{-1} is existent. To avoid Smith orthogonalization, let $\lambda_i(r,t) = L^*\vartheta_i(r,t)$, $\vartheta_i(r,t) = R_{(r_i,t_i)}(r,t)$, solve the equation $B\cdot[\zeta_1,\zeta_2,\ldots]^{\mathrm{T}} = [\lambda_1(r,t),\lambda_2(r,t),\ldots]^{\mathrm{T}}$, so the matrix $B = (L\lambda_i(r,t)|_{(r,t)=(r_j,t_j)})_{i,j=1,2,\ldots}$ is given, when B^{-1} is existent, the matrix $(L\zeta_j(r,t)|_{(r,t)=(r_i,t_i)})_{i,j=1,2,\ldots}$ is an identity matrix, so the analytical solution of Eqs. (5)–(7) is

$$Y(r,t) = \sum_{j=1}^{\infty} f(r_j,t_j,Y(r_j,t_j))\zeta_j(r,t),$$

the approximate solution of Eqs. (5)–(7) is

$$Y_m(r,t) = \sum_{j=1}^{m} f(r_j,t_j,Y(r_j,t_j))\zeta_j(r,t).$$

The proof processes are given in Ref. [16]. The approximate solution of Eqs. (1)–(3) is

$$\Phi_m(r,t) = Y_m(r,t) - Z(r,t).$$

If we use the TRHKM to solve the TFTE, the numerical solutions are not accurate. Therefore, we improve the TRHKM by extending the single piecewise interpolation to double piecewise interpolation. The steps are as follows:

(i) We extend the single piecewise interpolation to double piecewise interpolation. We believe that if the solution region is divided into n intervals, for each interval, using the TRHKM to calculate after stretching the interval, then restoring the stretched interval, the problem will become smoother and the numerical solution will be more accurate. First, let $d = 1/n$, $r_i = i\cdot d$, $t_i = i\cdot d$, $i = 0,1,2,\ldots,n-1$, so $\Omega = [0,1]\times[0,1]$ is divided into $\Omega_{i+1} = [r_i,r_{i+1}]\times[t_i,t_{i+1}]$. Second, stretch Ω_1 to Ω, using TRHKM to work out the $Y_{m,1}(r,t)$, which is the initial condition of Ω_2, stretch Ω_2 to Ω, using TRHKM to work out the $Y_{m,2}(r,t)$, which is the initial condition of $\Omega_3,\ldots$, until work out the $Y_{m,n}(r,t)$.

(ii) However, the accompanying issue is that while a higher number of partitions improves computation accuracy, it simultaneously increases the computational workload, resulting in longer computation time. In fact, it is observed that the numerical errors obtained from $n = 1000$ and $n = 100$ are similar. But the computational effort of the former is much larger

than the latter. For instance, the smooth "**+**" region in Fig. 1, a large number of partitions do not enhance the precision of the numerical solution. Therefore, we consider that how to choose d rationally to ensure both accuracy and time efficiency.

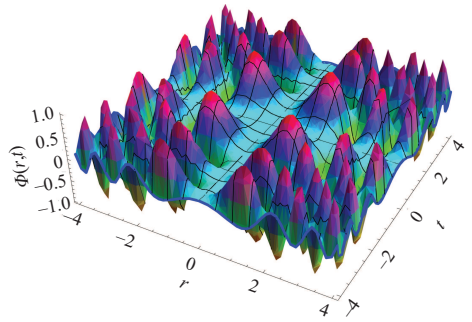


Fig. 1. The smooth "**+**" region.

To solve this problem, we use the means of combining adaptive techniques. We establish a fixed threshold δ to limit the number of partitions: when the absolute errors exceed δ, we continue partitioning. And when the absolute errors fall below δ, we stop partitioning. As shown in Fig. 2, the n is automatically selected with more nodes for computation in steep regions. To enhance computational accuracy, we stretch the domain and restore the domain after the computation.

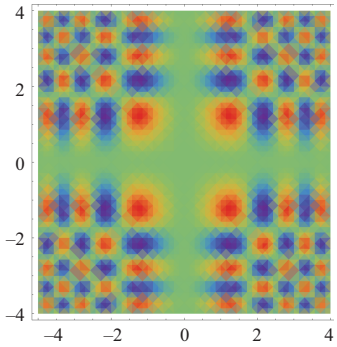


Fig. 2. The interval n is automatically selected with more nodes for computation in steep regions.

Theorem 1 (Convergence analysis) If $\Phi_n(r,t) \xrightarrow{\|\cdot\|} \Phi(r,t)(n\to\infty)$, then $\Phi_n(r,t)\to\Phi(r,t)(n\to\infty)$.

Proof For $\forall\ (r,t)\in\Omega$,

$$|\ \Phi_n(r,t)-\Phi(r,t)\ |=|\ \left\langle \Phi_n(\xi,\eta)-\Phi(\xi,\eta), R_{(\xi,\eta)}(r,t)\right\rangle\ |\le \|\ \Phi_n(\xi,\eta)-\Phi(\xi,\eta)\ \|\|\ R_{(\xi,\eta)}(r,t)\ \|, \tag{8}$$

where $R_{(\xi,\eta)}(r,t)$ is the RK of $H(\Omega)$. $\exists\ P>0$, it has

$$|\ \Phi_n(r,t)-\Phi(r,t)\ |\le P\ \|\ \Phi_n(\xi,\eta)-\Phi(\xi,\eta)\ \|\ . \tag{9}$$

Because $\Phi_n(\xi,\eta) \xrightarrow{\|\cdot\|} \Phi(\xi,\eta)(n\to\infty)$, $\Phi_n(r,t)\to\Phi(r,t)(n\to\infty)$. □

Theorem 2 (Error estimate) If $\Phi_m(r,t)$ is the approximate solution, $\Phi(r,t)$ is the analytical solution, $d=|r_{i+1}-r_i|=|t_{i+1}-t_i|$, then a positive constant ε exists such as

$$\|\Phi(r,t)-\Phi_m(r,t)\|_\infty=\max\ |\Phi(r,t)-\Phi_m(r,t)|\ \le\varepsilon h^2,\ (r,t)\in[0,1]\times[0,1], \tag{10}$$

where $h=\max\{d_1/m,\ d_2/m,\ldots,d_n/m\}$.

Proof For the sake of proof, after stretching the interval, (r,t) turns into (p,q). A positive constant ε exists such as

$$\|\Phi(p,q)-\Phi_{1,m}(p,q)\|_\infty=\max\ |\Phi(p,q)-\Phi_{m,1}(p,q)|\ \le\varepsilon {h_1}^2,\ (p,q)\in\Omega_1, \tag{11}$$

where $h_1=\max\{d_1/m\}$.

A positive constant ε exists such as

$$\|\Phi(p,q)-\Phi_{2,m}(p,q)\|_\infty=\max\ |\Phi(p,q)-\Phi_{m,2}(p,q)|\ \le\varepsilon {h_2}^2,\ (p,q)\in\Omega_2, \tag{12}$$

where $h_2=\max\{d_1/m,\ d_2/m\}$.

...

A positive constant ε exists such as

$$\|\Phi(p,q)-\Phi_{n,m}(p,q)\|_\infty=\max\ |\Phi(p,q)-\Phi_{n,m}(p,q)|\ \le\varepsilon {h_m}^2,\ (p,q)\in\Omega_m, \tag{13}$$

where $h_m=\max\{d_1/m,\ d_2/m,\ldots,d_n/m\}$. Then restoring the stretched interval (p,q) to (r,t). Hence, $\|\Phi(r,t)-\Phi_m(r,t)\|_\infty\le\varepsilon h^2$, where $h=\max\{d_1/m,\ d_2/m,\ldots,d_m/n\}$. □

4. Experiments

In this part, three numerical experiments and a simulation are presented to validate the applicability and efficiency of the ADPIRHKM. To this end, all parameters are carefully selected to ensure computational accuracy and efficiency.

Experiment 1 Consider the following β-th TFTE[1,17]

$$\frac{\partial^{\beta}\Phi(r,t)}{\partial t^{\beta}}+\frac{\partial^{\beta-1}\Phi(r,t)}{\partial t^{\beta-1}}+\Phi(r,t)=\frac{\partial^{2}\Phi(r,t)}{\partial r^{2}}+\left(\frac{2t^{-\beta}}{\Gamma(4-\beta)}+\frac{2t^{1-\beta}}{\Gamma(5-\beta)}+4\pi^{2}+1\right)t^{3}\sin(2\pi r).$$

In Eqs. (2) and (3), $\varphi(r)$, $\psi(r)$, and $\hbar(t)$ can be obtained from the analytic solution $\Phi(r,t)=t^{3}\sin(2\pi r)$. Let $n=500$, $d=0.002$, $\delta=10^{-4}$, $\beta=1.2$, $L_{\infty}=|\Phi(r_j,t_j)-\Phi_m(r_j,t_j)|$ is the absolute error norm, by Wolfram Mathematica, Table 1 shows the maximum L_{∞} of the local discontinuous Galerkin method (LDGM),[17] meshfree spectral approach (MSA),[1] TRHKM,[16] AMPIRKM,[15] and ADPIRHKM at $t=1$. Figure 3 shows the L_{∞} by TRHKM (a), AMPIRKM (b), and ADPIRHKM (c). By comparing Fig. 3, we can see that the ADPIRHKM provided in this paper is more accurate.

Table 1. Maximum L_{∞} of Experiment 1 for $\beta=1.2$, $n=500$, and $d=0.002$ at $t=1$.

	LDGM[17]	MSA[1]	TRHKM[16]	AMPIRKM[15]	ADPIRHKM
L_{∞}	5.3939×10^{-4}	3.1158×10^{-4}	0.917485	6.50073×10^{-3}	4.75779×10^{-5}

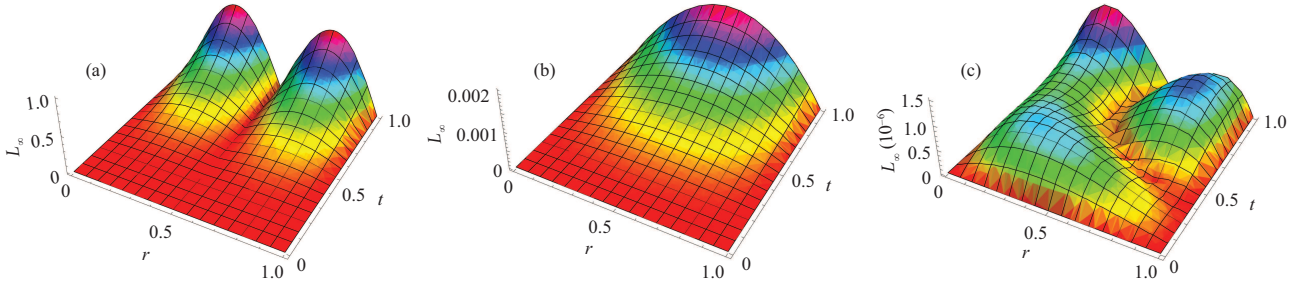


Fig. 3. L_{∞} of Experiment 1 by TRHKM (a), AMPIRKM (b), and ADPIRHKM (c) for $\beta=1.2$, $n=500$, and $d=0.002$.

Experiment 2 Consider the following β-th TFTE[3]

$$\frac{\partial^{\beta}\Phi(r,t)}{\partial t^{\beta}}+\frac{\partial^{\beta-1}\Phi(r,t)}{\partial t^{\beta-1}}+\Phi(r,t)=\frac{\partial^{2}\Phi(r,t)}{\partial r^{2}}+\left(\frac{\Gamma(2)}{\Gamma(3-\beta)}t^{2-\beta}+t\right)(r^{2}-r)-2t.$$

In Eqs. (2) and (3),

$$\varphi(r)=0,\quad \psi(r)=r(r-1),$$
$$\hbar(0,t)=\hbar(1,t)=0,\quad \Phi(r,t)=(r^{2}-r)t.$$

Let $\beta=1.5$, $n=1000$, $d=0.001$, $\delta=10^{-4}$.

Table 2 shows the L_{∞} by using the above two methods. By comparison with the AMPIRKM and ADPIRHKM methods, we can see that the ADPIRHKM provided in this paper is more accurate.

Table 2. L_{∞} of the two methods for $\beta=1.5$, $n=1000$. and $d=0.001$.

(r,t)	Exact solution	AMPIRKM[15]	ADPIRHKM
(0.1,0.1)	−0.009	9.00724×10^{-5}	8.99973×10^{-6}
(0.2,0.2)	−0.032	3.19877×10^{-4}	3.20814×10^{-6}
(0.3,0.3)	−0.063	6.30129×10^{-4}	6.29981×10^{-6}
(0.4,0.4)	−0.096	9.59766×10^{-4}	9.60324×10^{-6}
(0.5,0.5)	−0.125	1.25039×10^{-3}	1.25043×10^{-6}
(0.6,0.6)	−0.144	1.44005×10^{-3}	1.43996×10^{-6}
(0.7,0.7)	−0.147	1.47046×10^{-3}	1.47013×10^{-6}
(0.8,0.8)	−0.128	1.28022×10^{-3}	1.28008×10^{-5}
(0.9,0.9)	−0.081	8.11051×10^{-4}	8.10902×10^{-5}

Experiment 3 Consider the following β_i and α_i TFTE and its initial and boundary conditions[2]

$$\frac{\partial^{\beta_1}\Phi(r,t)}{\partial t^{\beta_1}}+\frac{\partial^{\beta_2}\Phi(r,t)}{\partial t^{\beta_2}}+2\left(\frac{\partial^{\alpha_1}\Phi(r,t)}{\partial t^{\alpha_1}}+\frac{\partial^{\alpha_2}\Phi(r,t)}{\partial t^{\alpha_2}}\right)+\Phi(r,t)=\frac{1}{2}\frac{\partial^{2}\Phi(r,t)}{\partial r^{2}}+g(r,t).$$

In Eqs. (2) and (3), $\varphi(r) = \mathrm{e}^{-r}\cdot\sin r$, $\psi(r) = -\mathrm{e}^{-r}\cdot\sin r$, $\hbar(0,t) = 0$. $g(r,t)$ can be obtained from the analytic solution $\Phi(r,t) = \mathrm{e}^{-t-r}\cdot\sin r$. Let $n = 1000$, $d = 0.001$, $\delta = 10^{-4}$. Table 3 shows the L_∞ by three methods for $\beta_1 = 1.9$, $\beta_2 = 0.9$, $\alpha_1 = 1.85$, $\alpha_2 = 0.85$, and $\beta_1 = 1.7$, $\beta_2 = 0.7$, $\alpha_1 = 1.55$, $\alpha_2 = 0.55$. For $(8,8)$ and $(10,10)$ cases, although the numerical solution obtained by the ADPIRHKM is slightly less accurate than that from the Romanovski–Jacobi polynomials,[2] it demonstrates superior stability across the entire domain.

Table 3. Comparisons of L_∞ of Experiment 3.

(β_1,β_2)	(α_1,α_2)	Methods	(6,6)	(8,8)	(10,10)
(1.9,0.9)	(1.85,0.85)	Romanovski–Jacobi polynomials[2]	3.08890×10^{-4}	7.97130×10^{-7}	1.93870×10^{-7}
		AMPIRKM[15]	1.81183×10^{-3}	4.52424×10^{-3}	9.11866×10^{-3}
		ADPIRHKM	9.84788×10^{-5}	2.44935×10^{-6}	4.91720×10^{-6}
(1.7,0.7)	(1.55,0.55)	Romanovski–Jacobi polynomials[2]	7.02340×10^{-4}	5.87170×10^{-7}	1.58650×10^{-7}
		AMPIRKM[15]	1.81364×10^{-3}	4.52877×10^{-3}	9.12778×10^{-3}
		ADPIRHKM	9.83279×10^{-5}	2.44559×10^{-6}	4.90960×10^{-6}

5. Numerical simulation

Consider the following influence of β on neutron flux TFTE for graphite[3,18]

$$\frac{\tau}{\upsilon}\frac{\partial^\beta \Phi(r,t)}{\partial t^\beta} + \tau(B-\Sigma)\frac{\partial^{\beta-1}\Phi(r,t)}{\partial t^{\beta-1}} + (B-\Sigma)\Phi(r,t) = D\frac{\partial^2\Phi(r,t)}{\partial r^2} + g(r,t),$$

with initial conditions

$$\varphi(r) = 0,\ \psi(r) = 0, \tag{14}$$

and boundary conditions

$$\hbar(0,t) = 0,\ \ \hbar(1,t) = t^3\sin(1), \tag{15}$$

where

$$g(r,t) = \left(3\frac{\Gamma(3)}{\Gamma(4-\beta)}t^{3-\beta} + 3\frac{\Gamma(3)}{\Gamma(5-\beta)}t^{4-\beta} + t^3\right)\sin^2(r) - 2\pi t^3\cos(2r).$$

Let $\tau = 1$, $\nu = 1$ m/s, $B = 1.00032$, $D = 3.141$ cm. Diffusion parameters of graphite $\Sigma = 0.00032$.

Table 4 gives the comparison of maximum L_∞ with $\beta = 1.15$, 1.35, 1.55, 1.75, and 1.95 by Fibonacci–Wavelet method ($M = 4$),[3] Legendre–Wavelet method ($M = 4$),[3] AMPIRKM,[15] and ADPIRHKM ($\delta = 10^{-5}$, $h = 0.0001$, and $n = 10000$). Obviously, we can see that the ADPIRHKM provided in this paper is more precise. The values of β considered for the computation are $\beta = 1.1$, 1.3, 1.5, 1.7, and 1.9. $\delta = 10^{-4}$, $h = 0.001$, and $n = 1000$.

Figure 4 shows the neutron flux for graphite with $\beta = 1.1$, $\beta = 1.5$, and $\beta = 1.9$ at $t = 1$ s. In Fig. 4, for different β, the neutron flux for graphite is different. As t increases, the neutron flux of graphite decreases. This indicates that the lower the neutron density in the reactor, the slower the rate of the chain reaction and the lower the power output of the reactor. When $r = 3$ cm, the neutron flux is close to zero. The neutron flux being too low may cause the reactor to be unable to sustain the chain reaction, or even lead to a shutdown. Insufficient power output would fail to meet energy demands.

Figure 5 presents the error function at $t = 1$ for different β of by the method reported in Ref. [18]. Figure 6 shows L_∞ at $t = 1$ for different β by ADPIRHKM. It is observed that the error value is increasing when β is arising.

Table 4. Comparisons of the maximum L_∞ by four methods.

β	Fibonacci–Wavelet[3]	Legendre–Wavelet[3]	AMPIRKM[15]	ADPIRHKM
1.15	6.4346×10^{-6}	7.5593×10^{-6}	6.36377×10^{-4}	6.56041×10^{-7}
1.35	6.3611×10^{-6}	7.3935×10^{-6}	9.65800×10^{-3}	8.19133×10^{-7}
1.55	5.8519×10^{-6}	7.1980×10^{-6}	7.24024×10^{-3}	7.20247×10^{-6}
1.75	6.8947×10^{-6}	6.9749×10^{-6}	2.09721×10^{-3}	6.56041×10^{-6}
1.95	6.2791×10^{-5}	6.6688×10^{-6}	2.94118×10^{-3}	8.99967×10^{-6}

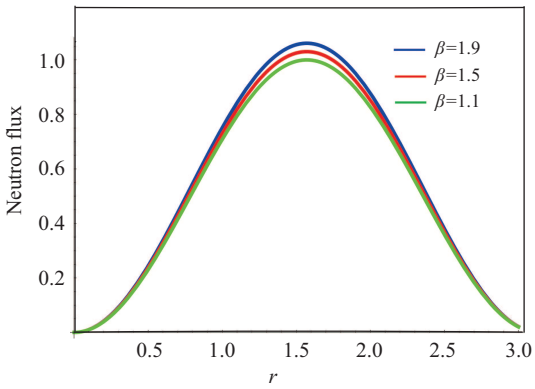


Fig. 4. Neutron flux of graphite with $\beta = 1.1$, $\beta = 1.5$, and $\beta = 1.9$ at $t = 1$ s.

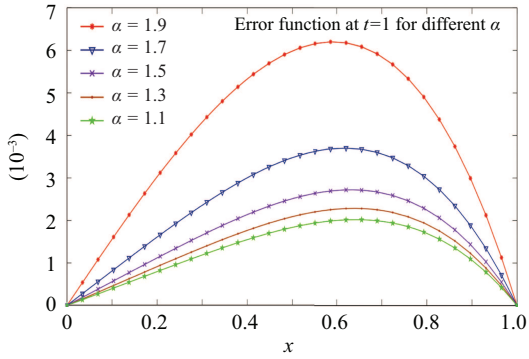


Fig. 5. L_∞ for neutron flux of graphite with $\beta = 1.1$, 1.3, 1.5, 1.7, and 1.9 by method reported in Ref [18] at $t = 1$ s.

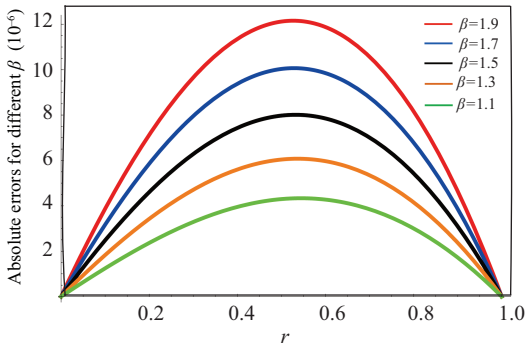


Fig. 6. L_∞ for neutron flux of graphite with $\beta = 1.1$, 1.3, 1.5, 1.7, and 1.9 by ADPIRHKM at $t = 1$ s.

6. Conclusions

In this paper, TRHKM is improved. First, we produce a sparse matrix B by selecting the appropriate parameters, avoiding to calculate conjugate operator and practise Gram–Schmidt orthogonalization. Second, the ADPIRHKM is proposed to solve the model of the neutron transport process in the nuclear reactor core, which combines the technology of adaptive and double piecewise interpolation. The adaptive multi-step technique makes the piecewise number more reasonable, and the double piecewise interpolation means makes the absolute errors more accurate. The interpolation facilitates a smoother problem configuration. Then, three numerical experiments show that the improved method is a highly effective numerical method. Last, the numerical simulation shows the effect of time t and β on the neutron flux behavior of graphite. This paper has provided a new numerical calculation method in the field of dynamics of neutron flux in a nuclear reactor.

Acknowledgments

Project supported by the National Natural Science Foundation of China (Grant No. 12262024), the Autonomous Region Directly Affiliated University Basic Research Business Expenses Project (Grant Nos. NCYWT23023, NCYWT23043, NCYWT23034, and NCYWS25019), the Natural Science Foundation of Inner Mongolia Autonomous Region, China (Grant Nos. 2026MS0186, 2024MS07012, and 2024LHMS06013), the "Supporting Project for Young Scientific Technological Talents" of Colleges and Universities of Inner Mongolia Autonomous Region, China (Grant No. NJYT23097), the Special Project for First-Class Discipline Research of the Department of Education of Inner Mongolia Autonomous Region, China (Grant No. YLXKZX-NCD-001), the Fund from the Research Center for Regional Digital Economy and Digital Governance, and the Research Project of Inner Mongolia Key Laboratory of Economic Data Analysis and Mining (Grant No. SY25014).

References

[1] Nikan O, Avazzadeh Z and Tenreiro Machado J A 2021 *Nonlinear Sci. Numer. Simulat.* **99** 105755
[2] Nazari J, Heydari M H and Hosseininia M 2023 *Result Phys.* **53** 106937
[3] Singh U 2022 *Results Control. Optim.* **9** 100180
[4] Abdulazeez S T and Modanli M 2022 *Alex. Eng. J.* **61** 12443
[5] Kapoor M 2024 *Ain. Shams. Eng. J.* **15** 102922
[6] Hong Z, Wang Y J and Hao H 2019 *J. Comput. Appl. Math.* **345** 405
[7] Yuzbas S 2016 *Appl. Math. Comput.* **287–288** 83
[8] Zogheib B and Tohidi E 2018 *Comput. Math. Appl.* **75** 3571
[9] Sharma S, Bala A and Aeri S 2024 *Partial. Differ. Equations Appl. Math.* **11** 100770
[10] Hesameddini E and Asadolahifard E 2016 *Comput. Math. Appl.* **72** 1926
[11] Mamadu E J, Ojarikre H I and Iweobodo D C 2024 *Sci. Afr.* **26** e02486
[12] Qiu R, Xu M and Zhu P 2025 *Appl. Math. Comput.* **489** 219161
[13] Attia N, Akgul A and Seba D 2022 *Result. Phys.* **35** 105225
[14] Momani S, Djeddi N and Al-Smadi M 2021 *Appl. Numer. Math.* **170** 418
[15] Du M J, Sun B J and Kai G 2023 *Chin. Phys. B* **32** 030202
[16] Wang Y L and Su L J 2011 *Comput. Math. Appl.* **61** 421
[17] Wei L, Liu L and Sun H 2018 *Taiwan J. Math.* **22** 1509
[18] Hosseini V R and Chen W Z 2014 *Eng. Anal. Bound. Element* **38** 31
[19] Roul P, Rohil V and Espinosa-Paredes G 2023 *Ann. Nucl. Energy* **185** 109733